Investigating many-electron exchange effects in electron–heavy-atom scattering

S. Bellm,[1] J. Lower,[1] Z. Stegen,[2] D. H. Madison,[2] and H. P. Saha[3]
[1]*AMPL, Research School of Physical Sciences and Engineering, Australian National University, Canberra, ACT 0200, Australia*
[2]*University of Missouri–Rolla, 1870 Miner Circle, Rolla, Missouri 65409-0640, USA*
[3]*University of Central Florida, Orlando, Florida 32816-2385, USA*
(Received 5 December 2007; published 25 March 2008)

In a recent publication we presented measurements and distorted-wave Born approximation (DWBA) calculations for spin asymmetries resulting from the scattering of 148 eV spin-polarized electrons from ground-state xenon atoms. While achieving reasonably good agreement between theory and experiment by accounting for many-body exchange effects through a local exchange potential, sizable discrepancies remained in some cases. It was proposed that a more sophisticated treatment of exchange might be the key to obtaining better agreement. Here we present high-precision experimental results at a lower projectile-electron energy of 112 eV. Due to improvements made to our spectrometer, these data are of significantly-improved statistical accuracy over those obtained previously. They are compared to DWBA calculations, within whose framework electron exchange is treated in three different ways. In the first, only exchange between the projectile electron and ejected target electron is considered and that between the continuum- and bound-electrons is ignored. In the second, exchange between the continuum- and bound-electrons is treated through a local approximation. Finally, exchange is included through a Hartree-Fock (HF) calculation of wave functions for both bound- and continuum-electrons. While this more sophisticated treatment of exchange narrows the gap between experiment and theory, the results suggest improvements in other aspects of the problem may be warranted.

DOI: 10.1103/PhysRevA.77.032722 PACS number(s): 34.80.Dp, 34.80.Nz

I. INTRODUCTION

A. Motivation

The provision of accurate atomic-collision cross sections is important for a wide variety of modeling applications, ranging from the physics and chemistry of the upper atmosphere, optimization of lasers, and more recently [1,2] investigations into the development of nonmercury gas discharges for lighting. Furthermore, the explication of mechanisms underlying atomic collision processes may lead to the development of models linking disparate area of physics and chemistry and inspire the conception of new technologies. The purpose of this study is to improve our understanding of the ionization of heavy atoms by electron impact through elucidating the role of many-electron exchange effects.

The ionization of both light- and heavy-atomic species by electron impact has proven to be a severe theoretical challenge over many decades. Even today for the low-Z electron-helium system at low- to intermediate-energies, significant discrepancies with experiment have been recently reported for out-of-plane scattering [3] and for cases where the residual ion is left in an excited state [4]. For ionization of heavier atoms, the situation is more complex. The simplest viable theory for this case is the distorted wave Born approximation (DWBA). While DWBA calculations provide a favorable degree of agreement with experiment at higher continuum-electron energies, as the ionization threshold is approached larger disparities emerge. Here we restrict our study to the process of single ionization, which is the dominant ionization process at low- to intermediate-impact-energies. For heavy atomic targets, the description of electron-impact-induced ionization is complicated by two issues.

First, for atoms heavier than hydrogen, not only must the process of exchange between the projectile- and ejected-electron be treated, but also processes involving exchange between the continuum electrons (the projectile-, ejected-, and scattered-electron) and all remaining bound electrons in the atomic (ionic) system. The process of exchange between the continuum electrons and the atom (ion) has been previously referred to as "exchange distortion" and is treated in a distinctly different way than exchange between the projectile and ejected electron in the DWBA formalism. In the potential picture, "exchange distortion" can be conceived as the difference between the potential experienced by an electron, and that by a fictitious particle possessing the same mass and charge and traveling at an identical velocity and along an identical trajectory through the atomic (ionic) charge cloud. One way of partially accounting for exchange distortion is through the inclusion of a local-exchange potential, such as developed by Furness-McCarthy [5]. This was the approach adopted in our previous publication [6]. However, to treat many-body exchange-processes properly requires the nonlocal character of exchange to be taken into account. Here we perform more sophisticated calculations in which the Hartree-Fock (HF) method is used to calculate wave functions for the continuum electrons. In this way, within the DWBA formalism, we treat exchange (and polarization) effects much better than previously. Details of these calculations and comparison with those using the Furness-McCarthy potential are presented in Sec. III.

Second, the importance of relativistic effects in electron-atom scattering increases rapidly with increasing atomic number. Whereas for light atoms relativistic effects can be accounted for through angular-momentum coupling, for scattering from heavy atoms the influence of relativity on the bound-state wave functions and continuum wave functions, describing the atom (ion) and the continuum electrons, respectively, needs to be addressed. For the case of heavy atomic targets at low- to medium-impact-energies, experiments involving the scattering of spin-polarized electrons

have revealed the effects of explicit spin-dependent forces acting on the trajectories of the elastically scattered electrons [7,8]. Furthermore, earlier work on ionization of xenon atoms revealed that the experimentally-determined branching ratio, describing excitation to the $5p^5\ ^2P_{1/2}$ and $5p^5\ ^2P_{3/2}$ residual-ion states, could only be accurately described by employing relativistic bound-state wave functions for the residual ion [9]. In contrast, comparison of experimentally-derived spin-asymmetry data for the same system with non-, semi-, and fully-relativistic calculations suggested that a nonrelativistic scattering theory was sufficient to describe this quantity. Nevertheless, while significant disparity between experiment and theory persists, the contribution of relativistic effects remains unclear.

For reaction kinematics where the energies of the projectile-, scattered-, and ejected-electrons are high, DWBA calculations normally yield relatively good agreement with the experimental data [10–12]. Under such conditions, a number of physical effects can be neglected to improve the tractability of calculation with little loss of accuracy. First, nonlocal aspects of exchange between the continuum- and bound-state-electrons can be neglected and an approximate local exchange potential employed. Second, under these conditions of short interaction time between the continuum electrons and the atom (ion), the degree of charge-cloud polarization is rendered small, enabling both the atom and ion to be accurately described by a static potential. Together these approximations constitute the so-called "static-exchange approximation." While appropriate to high-energy electrons, this approximation breaks down at low energies.

In this work we again focus on the so-called spin-asymmetry function. Studies of this quantity allow contributions to the ionization process from many-electron exchange processes [6], which contribute strongly at low energies, and relativistic effects [13] to be isolated and sensitively tested. In contrast to our recent work [6], the present measurements are performed at a lower impact energy and for equal energies of the two final-state continuum electrons. It was anticipated that these new kinematics (in particular the lower impact energy) would enhance the very exchange effects whose description we were seeking to improve. Enhancements to our experimental apparatus have also been wrought, leading to data of greatly-improved statistical accuracy. On the theoretical side, more sophisticated tools are now applied. In particular, HF calculations for the continuum electrons have been performed to account for the nonlocal character of the many-electron exchange process and the effects of charge-cloud polarization.

The most detailed information on single-ionization dynamics comes from measurements performed within a kinematically complete framework [14]. To this end we employ the $(e,2e)$ electron coincidence technique to determine the respective momenta ($\mathbf{p}_1$ and $\mathbf{p}_2$) and energies (E_1 and E_2) of the two final-state continuum electrons. Combined with knowledge of the projectile electron momentum $\mathbf{p_i}$ (energy E_i), the recoil momentum of the ion $\mathbf{q}$ and the binding energy ε of the ejected target electron can then be determined through the energy and momentum conservation relations:

$$\mathbf{q} = \mathbf{p}_i - \mathbf{p}_1 - \mathbf{p}_2, \tag{1}$$

$$\varepsilon = E_i - E_1 - E_2. \tag{2}$$

This paper concerns the electron-impact-induced ionization of ground-state xenon atoms by spin polarized electrons to the energetically-resolved $Xe^+\ 5p^5\ ^2P_{1/2}$ and $5p^5\ ^2P_{3/2}$ fine-structure levels. In detail the reaction considered is

$$e^-(E_i)(\uparrow\downarrow) + \mathrm{Xe}\ 5p^6(^1S_0) \rightarrow \mathrm{Xe}^+5p^5(^2P_{1/2},^2P_{3/2}) + e^-(E_1) + e^-(E_2). \tag{3}$$

Here, $\uparrow$ or $\downarrow$ represent either positive ($m_s=+1/2$) or negative values ($m_s=-1/2$) of spin-projection quantum number for the electron initiating the ionizing collision.

B. Background

In our earlier publication [6] we reviewed the history of spin-resolved $(e,2e)$ experiments and their theoretical treatment. To avoid unnecessary repetition, this discussion is largely restricted to recent developments in the scattering of spin polarized electrons from xenon atoms and how this system can be used to deduce information on the electron-impact-induced ionization of heavy targets in general.

The polarized-electron—xenon system is a particularly attractive candidate for studying ionization of heavy atoms for a number of reasons. First, its large 1.3 eV fine-structure splitting is easy to resolve experimentally. This is important as Hanne and co-workers [15] showed that in the nonrelativistic limit, by resolving the fine-structure ionic levels of a closed-shell (spin zero) atomic system, a strong spin dependence of the ionization cross section could be observed through a mechanism arising from exchange between the projectile electron and ejected target electron. Their analysis was performed under the *LS* coupling scheme. DWBA calculations were carried out employing the Furness-McCarthy exchange potential [5] in the calculation of the distorted waves. Their model showed that the spin dependence would vanish in the limit of vanishing amplitudes describing exchange between the two final-state continuum electrons. The work demonstrated that by studying such spin asymmetries, sensitive information on the magnitude and phase of amplitudes describing two-body exchange could be derived from experiment. Strong spin asymmetries were predicted and subsequently observed by experiment. That relativistic effects, not included in their model, might induce additional asymmetries was acknowledged.

Early calculations based on this model [16–20] were partially successful in describing the experimental results which were themselves limited in statistical accuracy. Improvements in theory were pursued through a number of avenues. The sensitivity of cross-section calculations on relativistic effects in the bound-states was explored by comparing results obtained respectively with Hartree-Fock wave functions and Dirac-Fock wave functions to describe the target and residual ion. While the adoption of Dirac-Fock wave functions brought significant improvement to the description of branching ratios to the Xe^+ fine-structure levels, the spin-asymmetry function was found to be insensitive to the particular choice of bound-state description. Later work clarified the mechanisms underlying the observed spin asymmetries

by finding that while exchange between the incident electron and ejected target electron is, in the nonrelativistic limit, a necessary condition to observe nonzero values, the magnitude of the asymmetries is strongly influenced by exchange between the totality of continuum electrons and bound-state electrons. Thus the measurement of spin asymmetries can be used to sensitively probe the nature of many-body exchange phenomena as well as two-body exchange phenomena in electron-atom scattering.

One open question is the extent to which explicit spin-dependent forces contribute to the measured spin asymmetries. Previous work [18,21] on intermediate-energy electron—xenon ionization experiments performed within a DWBA formalism indicates that a nonrelativistic scattering theory is probably sufficient to describe the process, at least for the case of valence shell ionization. In Guo *et al.* [9] calculations were performed with and without the inclusion of a real Pauli potential in the calculation of the distorted waves, allowing for the possibility of spin-flip processes in the entrance- and exit-channel for the continuum electrons. While some improvement in the description of the experimental data was achieved, subsequent deliberations questioned whether it provided an unambiguous signature for continuum relativistic effects. This view was supported by recent experimental work [22] on the ionization of the Ar $(2p)$ orbital which showed no significant modifications to the spin-asymmetry function due to manifestation of relativity. A similar conclusion was arrived at by Lechner *et al.* [23] who used a sophisticated density functional treatment of exchange to look at spin asymmetries in xenon, compared to the cruder local Furness-McCarthy exchange potential used in earlier work. They concluded that the apparent relativistic effects seen in [24] were exclusively the result of the choice of exchange potential used. Nevertheless, lack of a good agreement with experiment under certain conditions [25] still leaves this an open question.

In [6] we also explored the effects of postcollision interaction (PCI), namely the Coulomb interaction between the two continuum electrons in the final state, on the predicted spin-asymmetries. This was achieved by comparing DWBA with three-body distorted wave (3DW) calculations, the former taking account of PCI to first order only and the latter including it to all orders of perturbation theory. It was found, under the kinematics of the study, that the inclusion of PCI did not significantly affect the result of calculation, nor obviously reduce the remaining disparity between theory and experiment. In contrast, the addition of the local Furness-McCarthy exchange potential [5] into the DWBA calculation to account for exchange distortion brought significant improvement. In this paper we additionally compare results of measurement with those of a full Hartree-Fock calculation for both atomic- and projectile-electrons in which both exchange- and polarization-effects are carefully treated.

II. EXPERIMENT

A. Apparatus

A detailed description of the apparatus can be found in [8,26] so only a short account is presented here. Preferentially-longitudinally-polarized electrons are created by the photoexcitation of valence electrons from a strained gallium arsenide photocathode under illumination by circularly-polarized laser light. These electrons are subsequently extracted, deflected through 90°, and focused to form a transversely-polarized beam. Inversion of the beam polarization from into (spin down) to out of (spin up) the scattering plane (defined as the plane containing the projectile electrons and the measured ejected- and measured scattered-electrons) is achieved by reversing the helicity of the laser light via a liquid crystal retarder. The electron beam is subsequently transported to the main collision chamber in which two toroidal-sector electrostatic electron energy analyzers are housed. Inside this chamber it is decelerated to the experimental collision energy E_i and focused at a grounded interaction volume, defined by the overlap of electron and xenon beams. The latter is formed by effusion of xenon gas through a 1.0 mm internal-diameter tube orientated orthogonally to the scattering plane.

Electrons emitted within the scattering plane are momentum analyzed in one of the two analyzers located on opposite sides of the projectile electron beam. Each analyzer comprises a seven-element electrostatic lens system, four toroidal-sector electrodes, and a crossed-delay-line position-and-time-sensitive electron detector.

The purpose of the lens system is to select only those electrons emitted within a selected range of azimuthal emission angles $\Delta\alpha$ (measured out of the scattering plane), decelerate (or accelerate) them, and then focus them into the analyzer. In our previous measurement [6] the analyzers were operated with a slightly larger acceptance range $\Delta\alpha=2°$ leading to higher coincidence rates. However, the statistical quality of those measurements was degraded by the presence of a large stray-electron background resulting in increased uncertainty in the derived asymmetry data. For this work introduction of additional "antiscattering" apertures in the analyzers' electron optics and reduction of the size of their previously-installed apertures greatly suppressed the background level, at the small expense of reducing $\Delta\alpha$ from 2° to 1.4°. Details of the modified electron optics can be found in [26].

After passing through the electron optics, electrons are dispersed in space according to the magnitude and direction of their momenta leaving the interaction region. Their energy coordinates and scattering-angle coordinates (E_i,θ_i) are deduced from their arrival coordinates (x_i,y_i) at the detector. For the present experiment, each analyzer transmits electrons over an 8 eV range, with electron energies determined to an accuracy of 400 meV. $(e,2e)$ electron pairs are identified by measuring the relative arrival times of electrons at the two detectors. Random background events are subtracted using standard statistical techniques [27].

B. Data analysis

The measurement and data-analysis procedure is discussed in our earlier publication [6], so only a brief description will be presented here. The experiment consists of measuring $(e,2e)$ spin asymmetries for ionization of ground state

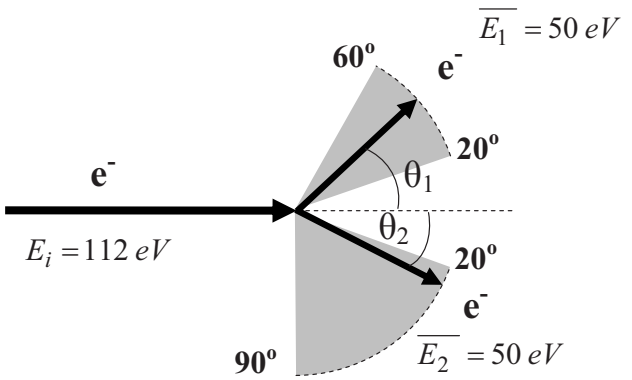

FIG. 1. Reaction kinematics. Single ionization is induced by a beam of spin-polarized electrons at an impact energy of 112 eV. Electrons of average energy $\bar{E}_1=50$ eV are detected to the left and to the right of the projectile electron beam, with the projectile electrons and the measured ejected- and scattered-electrons confined to a common plane (the scattering plane).

xenon atoms leading to the spin-orbit split Xe^+ $5p^5\ ^2P_{1/2}$ or $5p^5\ ^2P_{3/2}$ final-ion states. The reaction kinematics is shown in Fig. 1.

The energy E_i for the projectile electrons is 112 eV. Due to the difference in binding energies of the $P_{1/2}$ and $P_{3/2}$ states (13.44 eV and 12.13 eV, respectively), energy conservation, and the fixed-energy pass bands of the two analyzers, the reaction kinematics is as follows. For the $^2P_{3/2}$ state data is collected for $(e,2e)$ events where $45.3\ \text{eV}<E_j<53.3$ eV, $j=1,2$. For the $^2P_{1/2}$ state, the corresponding interval is $45.9\ \text{eV}<E_j<53.9$ eV. Both electron detectors collect electrons over a 40° range simultaneously. One detector is fixed to collect electrons over the range $20° \leq \theta_1 \leq 60°$ on the left of the incident beam. The second detector, located on the right side of the incident beam, is movable and can collect electrons over a 40° band, adjustable from outside of the scattering chamber, within the angular limits $20° \leq \theta_2 \leq 120°$. However, due to the greatly reduced coincidence rates at larger θ_2 values, data collection was restricted to $\theta_2 \leq 90°$ as indicated in Fig. 1.

Equation (2) is used to separate $(e,2e)$ events according to their final ion state $J=1/2$ or $J=3/2$. Spin asymmetries are calculated [6] through the equation

$$A_{J_i}(\theta_1,\theta_2) = \frac{1}{P_y}\frac{N_{J_i}^{\uparrow} - N_{J_i}^{\downarrow}}{N_{J_i}^{\uparrow} + N_{J_i}^{\downarrow}}. \tag{4}$$

Here $N_{J_i}^{\uparrow}$ and $N_{J_i}^{\downarrow}$ respectively represent count rates for positive- and negative-projections of spin (measured along the normal to the scattering plane) for the projectile electron instigating the ionization process and leading to the final ionic state J_i, $i=1/2,3/2$. $N_{J_i}^{\uparrow}$ and $N_{J_i}^{\downarrow}$ are determined by summing the counts under the corresponding energetically-resolved peaks in the binding-energy spectrum, formed by plotting $(e,2e)$ counts against binding energy ε, after random coincidence events have been subtracted. P_y is the component of the projectile-beam spin polarization along the normal to the scattering plane and was estimated to be $52\% \pm 3\%$ by measuring the up-down spin asymmetry in the elastic scattering of electrons from xenon at 50 eV [7].

To ensure that the experimental data would not be significantly affected by any apparatus-induced asymmetries, two additional measurements were made prior to the xenon $(e,2e)$ experiment. First, an accurate calibration of the angular scales of both analyzers was made. Second, asymmetries were measured on ground-state helium atoms where no measurable spin-dependent effects would be anticipated due to its low atomic number. A spin asymmetry value of zero was measured within statistical accuracy (0.1%), establishing that neither the position nor intensity of the primary-electron beam appreciably changed as its polarization was reversed. Finally, our $(e,2e)$ asymmetry data was checked for the condition $A_{J_i}(\theta_1,\theta_2)=-A_{J_i}(\theta_2,\theta_1)$ as required from parity considerations. Within statistical error, this was found to be true, giving us confidence that the measures taken had indeed been sufficient. However, the issue of quantifying and accounting for the effects of instrumental asymmetries is a nontrivial matter and dependent upon the particular experimental approach adopted. The reader is referred to Ref. [28] for a detailed discussion of such considerations.

It should be noted that for measurements involving position-sensitive detectors, such as the present, where different volumes of momentum phase space are mapped onto different spatial coordinates on the detector, the angular dependence of the asymmetry function can be determined much more accurately than that of the individual count rates $N_{J_i}^{\uparrow}$ and $N_{J_i}^{\downarrow}$ from which it is derived. This is because the effects of any position-dependent gain variations are removed through the ratio of Eq. (4). For this reason relative triple-differential cross sections are not presented here due to their inferior quality. However, recent developments in our experimental methodology [26] now allow us to measure relative triple-differential cross sections to a high accuracy. Such cross sections will appear in our future publications.

Resulting from the 400 meV analyzer energy resolution and the 300 meV energy width of the projectile electron beam, an $(e,2e)$ energy resolution of around 0.65 eV full width at half maximum (FWHM) was achieved. However, to improve statistics the asymmetries were calculated after performing an average of the $(e,2e)$ data over all combinations of E_1 and E_2 within the 8 eV acceptance bands of both analyzers. For an identical reason, an angular average over 2° intervals was performed in both θ_1 and θ_2. This, in combination with the ~2° in-plane angular resolution of both toroidal analyzers, translates into an effective angular resolution of 3° FWHM for electrons comprising $(e,2e)$ pairs.

III. THEORY

In this paper, the 3DW formalism [29] is applied to investigate the many-body nature of exchange in electron-atom scattering. The 3DW T matrix for direct scattering is given by

$$T_{fi}^{\text{3DW}} = \langle \chi_f \chi_{\text{eject}} C_{\text{proj-eject}} | V - U | \psi_{\text{active}} \chi_i \rangle. \tag{5}$$

Here ψ_{active} is the initial bound-state wave function for the active electron, χ_i (χ_f) is the initial (final) state distorted

wave for the projectile electron, χ_{eject} is the final-state distorted wave for the ejected electron, $C_{\text{proj-eject}}$ is the Coulomb interaction between the projectile- and ejected-electron (PCI), V is the initial-state interaction between the projectile- and neutral-atom, and U is a spherically-symmetric approximation for V. It is important to note that, in contrast to standard DWBA calculations [16] which only include PCI effects to first order, the 3DW approach accounts for PCI effects to all orders of perturbation theory.

In the DWBA formalism, exchange enters the calculation in two ways, namely through an exchange amplitude and through the calculation of the distorted waves. The exchange amplitude is identical in form to Eq. (6) except that the projectile electron is finally in state χ_{eject} and the ejected electron in state χ_f, i.e., the roles of projectile- and ejected-electrons are reversed. For high-energy calculations, the continuum wave function is found by solving the Schrödinger equation for some effective static local potential representing the atom or the ion. Such an approach [see Eq. (9) and associated discussion below] neither takes into account the polarization of the bound-state charge cloud by the continuum electrons nor the fact that the projectile can potentially exchange with any of the target electrons, not just the electron it ejects. While in the high-energy regime exclusion of such effects in calculation can be justified, neglecting them at low energies is likely to cause serious error. In contrast, in the Hartree-Fock method the equation for the continuum-electron distorted wave is solved self-consistently through the expression

$$(T_{\text{proj}} + U - k_i^2)\chi_i = \int V_{\text{ex}}(r,r')\chi_i^+(r')dr'. \tag{6}$$

Here T_{proj} is the kinetic energy operator and k_i^2 the energy of the projectile electron. U is the direct potential and V_{ex} is the nonlocal exchange potential that takes into account exchange between the projectile and all other electrons. This equation expresses the full nonlocal behavior of exchange, where the potential experienced by the projectile depends not only on its distance to each of the atomic electrons (on the charge density), but also on the phase of the scattering wave function over all space. Details of this approach have been described previously in the literature [30–34] so only a brief discussion will be given here.

In the Hartree-Fock method, the initial-state radial functions $P_l(r)$ for the continuum electrons are solutions of the equation

$$\left[\frac{d^2}{dr^2} + \frac{2Z}{r} - \frac{l(l+1)}{r^2}\right]P_l(r) = \frac{2}{r}[Y_l(r)P_l(r) + Q_l(r)] + \sum_{i'} \varepsilon_{ii'}P_{i'}(r). \tag{7}$$

Here Z is the nuclear charge and $\varepsilon_{ii'}$ are related to the Lagrange multipliers that ensure orthogonality. The screening potential is given by $(2/r)Y_l(r)$ and $(2/r)Q_l(r)$ is the exchange potential and $\varepsilon_{ii}=k_i^2$ is the kinetic energy of the continuum electron.

For the initial state, the projectile orbitals are calculated in the Hartree-Fock approximation with full exchange with the target electrons. As the initial state is described by an unrestricted Hartree-Fock calculation, the initial bound states contain the full effects of polarization by the projectile. For the final state, the Hartree-Fock continuum electrons are computed for an ion described within the frozen-core approximation, with the bound-state wave functions for the ion being fixed at the same self-consistent wave functions for the initial state. This implies a final-state core polarization equal to the initial-state core polarization, which is equivalent to assuming that the ionic core does not have time to relax during the process. Asymptotically, the incident electron is described by a phase-shifted plane wave and the final-state continuum electrons by phase-shifted Coulomb waves. Details of this calculation (subsequently labeled 3DW-HF) are presented in Ref. [29].

To gain greater insight into many-body electron-exchange processes in ionization and polarization effects at low-to-intermediate energies, additional calculations have been performed using a simplified treatment of exchange. In our second calculation (3DW-FM) exchange distortion is treated approximately by treating exchange between the continuum electrons and bound-state electrons as a local phenomenon, i.e., one which can be represented solely in terms of charge density. This was the approach adopted in our earlier publication [6]. In this case the nonlocal exchange potential $V_{\text{ex}}(r,r')$ of Eq. (8) is assumed to have a delta function behavior in the coordinate, resulting in the following approximation:

$$\int V_{\text{ex}}(r,r')\chi_i^+(r')dr' \approx U_{\text{ex}}(r)\chi_i^+(r'), \tag{8}$$

where $U_{\text{ex}}(r)$ is a local potential, approximating the true many-body exchange potential $V_{\text{ex}}(r,r')$. As a further approximation, the direct-scattering potential U is approximated by U_i, a *static* potential representing the atom and obtained from a Hartree-Fock calculation for an undistorted (unpolarized) isolated atom. Within this so-called "static exchange approximation", distorted waves are calculated through the equation

$$(T_{\text{proj}} + U_i - U_{\text{ex}} - k_i^2)\chi_i = 0. \tag{9}$$

In the present case we employ the static local exchange potential (FM) developed by Furness-McCarthy [5] of the form

$$U_{\text{ex}} = -\frac{1}{2}\{\sqrt{(\varepsilon_i - U)^2 + 4\pi\rho} - (\varepsilon_i - U)\}. \tag{10}$$

Here ε_i is the energy of the incident electron and ρ is the charge density for the initial-state neutral atomic-charge cloud. In this way an approximate account of exchange between the continuum electrons and bound state electrons is made. The triplet form of the FM approximation for U_{ex} is employed, where the charge density is half the full density for the atom (since the projectile can only exchange with an atomic electron of identical spin). Both final-state distorted waves are solutions of Schrödinger equations similar to Eq. (9) except that the neutral Hartree-Fock atomic potential U_i

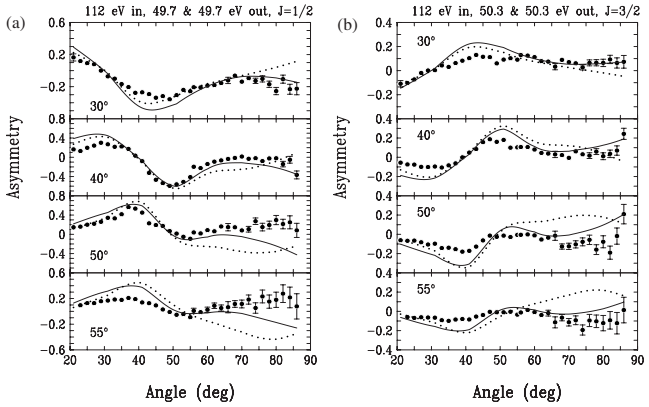

FIG. 2. Asymmetry data for ionizing transitions leading to (a) the Xe^+ $5p^5\ ^2P_{1/2}$ state and (b) the Xe^+ $5p^5\ ^2P_{3/2}$ ion state. The experimental results are compared with distorted-wave calculations neglecting exchange distortion (3DW, dotted line) and results from a full Hartree-Fock calculation (3DW-HF, solid line) which additionally accounts for exchange-distortion and polarization effects. The scattering angle θ_1 of the electron scattered to the left is fixed at the value indicated in each panel and the cross section is presented as a function of the scattering angle θ_2 for the second electron.

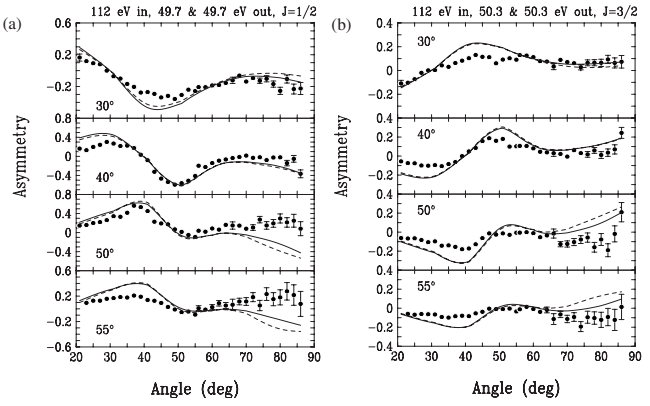

FIG. 3. Same experimental data and 3DW-HF calculation (solid line) as in Fig. 2 compared to the calculation employing the local Furness-McCarthy exchange potential (3DW-FM, dashed line) in which exchange distortion is approximately accounted for through the inclusion of a static local-exchange potential.

is replaced with the Hartree-Fock potential for the final-state ion U_{ion}. Thus, within the framework of this DWBA calculation, exchange distortion is treated approximately but no account is made for charge-cloud polarization of the atom or the ion.

Our third calculation (3DW) is carried out in a similar way to the second, except in this case exchange distortion is completely neglected and the distorted waves are calculated by setting the right-hand side of Eq. (6) to zero. In that case, the integro-differential equation simplifies to a pure differential equation of the form

$$(T_{\text{proj}} + U - k_i^2)\chi_i = 0, \tag{11}$$

where for the initial state U is the static potential for a neutral atom and for the final state U is the static potential for an ion. For this calculation, spin asymmetries can only arise from exchange between the projectile electron and the ejected target electron, as in the original model of Jones *et al.* [15], and polarization effects and exchange-distortion effects are neglected.

IV. COMPARISON OF THEORY WITH EXPERIMENT

Figures 2(a) and 2(b) compare the experimental results with 3DW calculations accounting for exchange between the projectile electron and ejected target electron only (no exchange distortion) and 3DW-HF calculations which include exchange between all continuum- and bound-electrons through Hartree-Fock wave functions.

Figure 2(a) corresponds to excitation of the $J=1/2$ ion state and Fig. 2(b) to excitation of the $J=3/2$ ion state. Statistical error bars are shown on the experimentally-derived data points when larger than the symbol (filled circle) used to represent them. Errors ($\sim$6%) relating to uncertainties in the measured value of the beam polarization are not shown on the figures.

The first thing to note is that the asymmetry function changes sign under the conditions of symmetric angles ($\theta_1 = \theta_2$) as it must from parity considerations (for equal angles and in the absence of spin analysis of the final state, the reaction viewed in a mirror plane orientated perpendicular to the scattering plane reverses the spin polarization of the incident beam but leaves the final state unchanged, i.e., the spin asymmetry must be identically zero). This behavior is reflected in both the experimental results and in the calculations. Good agreement is achieved between the 3DW-HF calculation and the experimental results concerning shape and magnitude of the asymmetry function. Although most calculated points lie outside the experimental error bars, that fact should be seen in the context that the experimental results have much improved precision over those presented previously [6] and therefore present a much more stringent test to theory. As would be anticipated, the 3DW calculations neglecting exchange distortion and polarization achieve a significantly poorer degree of agreement with the experimental data overall. This is particularly evident at larger values of the electron scattering-angles θ_1 and θ_2.

Figures 3(a) and 3(b) compare the same experimental results and 3DW-HF results as in Figs. 2(a) and 2(b) with a 3DW-FM calculation for which distorted waves are calculated using the local-exchange approximation of Furness-McCarthy [5]. This comparison facilitates exploration of the limitations of the static-exchange approximation. Under the present kinematics and at the smaller scattering angles θ_2, 3DW-FM and 3DW-HF calculations show minimum deviation from one another. At larger values of θ_2, only a small improvement in the degree of agreement between theory and experiment is achieved when 3DW-HF calculations are employed over 3DW-FM calculations. In light of the large improvements brought by the inclusion of a local exchange potential [Figs. 3(a) and 3(b)] and the small additional changes wrought by the full Hartree-Fock treatment, it appears that, for the present kinematics, the static-local-

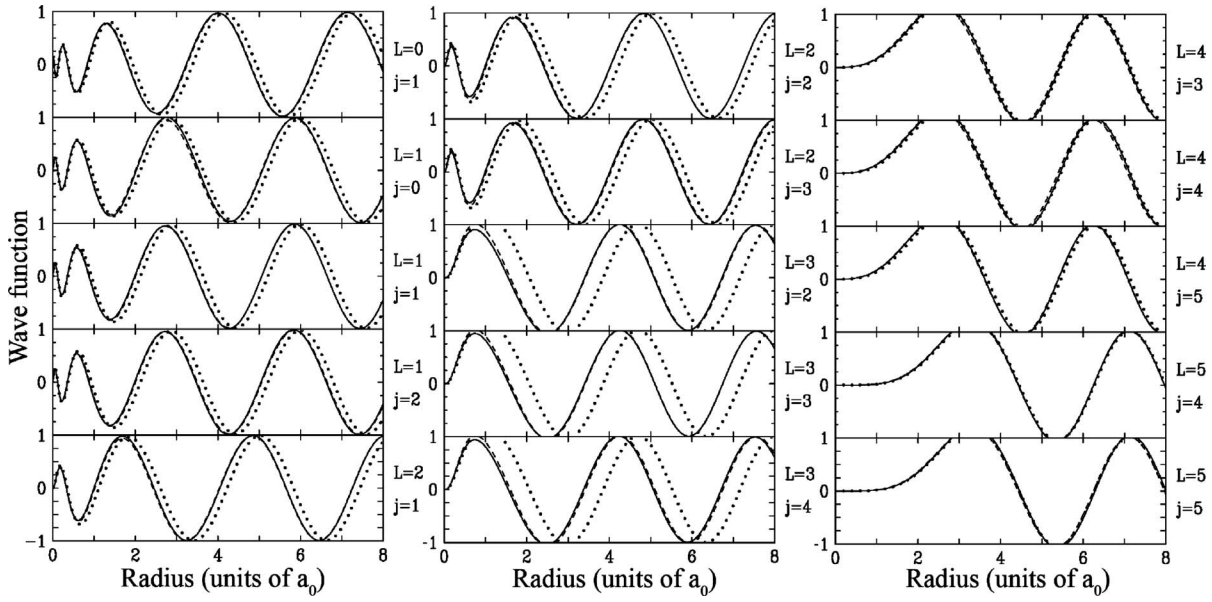

FIG. 4. Wave functions for the final-state continuum electrons calculated for the orbital-angular-momentum quantum-numbers $L=0$ to $L=5$ and for total angular momentum values for the electron—ion system of $J=L-1$, 0 and $L+1$ (ion angular momentum equals one). Results are presented as a function of distance from the nucleus. Calculations: 3DW (dotted line), 3DW-FM (dashed line), and 3DW-HF (solid line).

exchange approximation provides an accurate representation of the physics of exchange scattering and that the effects of atomic (ionic) charge-cloud polarization are small. Thus the origins of the remaining and, in certain angular regions, significant discrepancies between theory and experiment appear to lie elsewhere than in the details of the treatment of exchange.

To gain further insight into the influence of exchange and the way in which the static-exchange approximation breaks down, we compare in Fig. 4, plotted against units of Bohr radius (a_0), the associated partial waves calculated by the 3DW, 3DW-FM, and 3DW-HF calculations.

Results are presented for orbital angular momentum values for the continuum electrons of $L=0$ to $L=5$ and for values of total angular momentum for the electron—atom system of $J=L-1$, 0 and $L+1$. As expected, significant disparities are seen between partial waves calculated within the 3DW scheme (in which exchange distortion and polarization is ignored) and the partial waves calculated within the 3DW-FM and 3DW-HF approaches, peaking at $L=3$ and diminishing to negligible values by $L=5$. Interestingly, the almost imperceptible difference between the partial waves generated by the 3DW-FM and 3DW-HF calculations translates into much larger differences in the asymmetries to which they contribute at larger values of scattering angles θ_2 [see Figs. 3(a) and 3(b)]. This reflects the fact that cross sections are often very sensitive to details of the partial waves. A similar observation was made in [30,33] when comparing continuum waves calculated with the Hartree-Fock method with those calculated using the Furness-McCarthy approach for the ionization of the $3p$ shell of argon. In contrast to the present case, however, those calculations did not take into account the effect of the final-state electron—electron interaction which is included in the present, more sophisticated 3DW calculations.

Finally, to explore how the static-local-exchange approximation breaks down with decreasing continuum-electron energies, we plot in Fig. 5 individual partial waves for the Hartree-Fock and Furness-McCarthy calculations spanning orbital angular momentum values $L=0$ to $L=4$ and for the total angular momenta values $J=0$, $L-1$, and $L+1$. Calculations have been performed for equal-energy sharing between the two final-state continuum electrons at scattered-electron energies of 10, 20, 40, and 80 eV as a function of distance from the nucleus. Results begin at 30 a_0, by which distance the relative phases between the partial waves have converged. The following trends are observed. First, as the incident energy is lowered, deviations between the FM and HF partial waves increase. This is to be expected as at lower energies the nonlocal aspects of exchange become more pronounced and polarization effects are enhanced. Second, the largest differences are seen at the lowest energy of 10 eV for the classical total angular momentum $J=L-1$, with smaller deviations evident for the nonclassical $J=1$ and $J=L+1$ components. Interestingly, the largest differences are found for $L=2$.

V. CONCLUSION

We have presented experimental- and theoretical-results for the electron-impact-induced ionization of xenon atoms. The spin-asymmetry parameter, which provides a highly sensitive probe to investigate exchange effects in scattering, has been determined to high precision. In previous intermediate-impact-energy work on the electron—xenon system [6] we explored the sensitivity of scattering calculations on PCI and exchange distortion, the latter investigated by employing a local exchange potential. That work showed that calculation

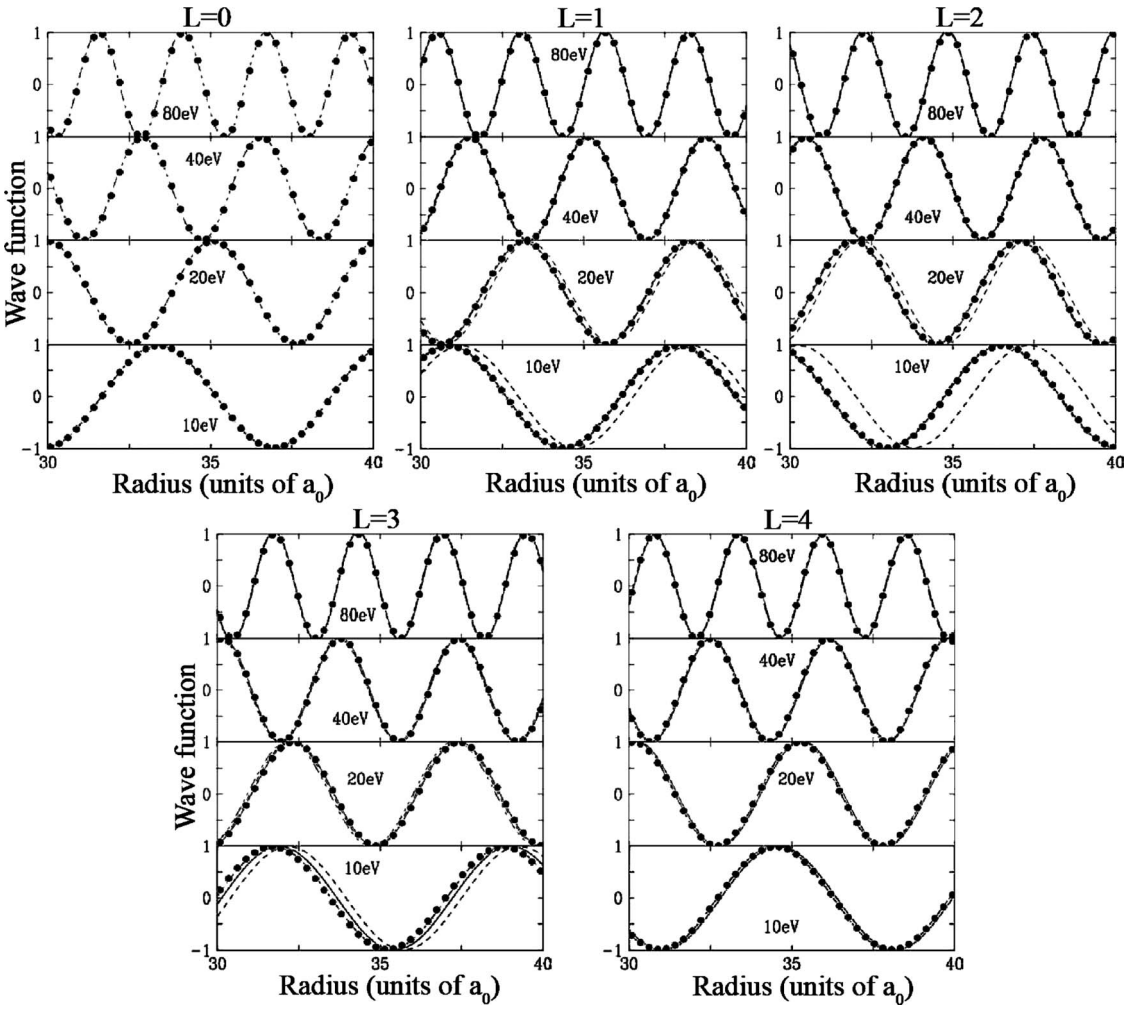

FIG. 5. Partial waves for two equal-energy final-state continuum electrons [3DW-FM (solid circles), 3DW-HF ($J=L-1$) (dash-dotted line), 3DW-HF ($J=L$) (solid line), and 3DW-HF ($J=L+1$) (dashed line)]. Calculations are presented for final-state continuum-electron energies of 10, 20, 40, and 80 eV. L is the orbital angular momentum of the continuum electron and J is the total angular momentum of the continuum electron plus residual ion with angular momentum unity.

was rather insensitive to PCI effects, but that significant improvements could be achieved through accounting for exchange distortion within the "static-exchange" approximation. However, the origins of the residual discrepancies between theory and experiment, which in some cases were quite large, remained unclear.

In this work we have presented experimental data of much higher precision and used it to test more sophisticated calculations in which exchange- and polarization-effects are accounted for by a full Hartree-Fock calculation for the bound- and continuum-electrons. The results show, as anticipated, that the more sophisticated treatment of exchange leads to an improved agreement with experiment, although the degree of improvement of this calculation over similar calculations employing the static-exchange approximation was not as great as expected.

To explore how the static-exchange approximation might perform as the energy of the continuum electrons is lowered, we have also presented calculations for the continuum-electron wave functions at lower continuum-electron energies. They predict a significant breakdown of the static-exchange approximation by 10 eV. To test this prediction, new experiments at low impact-energies are planned for the near future. Recent experimental developments now enable us to accurately correct for spatial variations in the electron-detection efficiency of our spectrometer. As a result, we will present high-precision spin-dependent relative triple-differential cross sections to accompany asymmetry data in the future, providing additional stringent tests to theory.

In light of the HF calculations in which exchange distortion and polarization are treated to high precision, the reasons for the remaining discrepancies between theory and experiment are still unclear. One possibility is a nonrelativistic treatment of electron—heavy-target scattering is inadequate, and that a relativistic treatment is required to describe the experimental data even at the present intermediate impact energies. Previous investigations all point away from this explanation. Nevertheless, to explore this we plan to incorporate relativistic continuum wave functions into the 3DW approach. Another possibility is channel coupling which was found to be important for ionization of argon [35] and which is not treated in our present approach. The electron-correlation effects and relativistic effects which are important in this case can be considered using the multichan-

nel Hartree Fock (MCHF) method [36] and Breit-Pauli approximation [35] in the initial-state wave function and the final state wave functions. Such a treatment might reduce the discrepancies between experiment and theory. We will pursue all these approaches in the future.

ACKNOWLEDGMENTS

We gratefully acknowledge the assistance of the Australian Research Council under Grant No. DP0452553 (S.B. and J.L.) and the United States National Science Foundation under Grant No. PHY-0070872 (Z.S. and D.H.M.).

[1] K. Bartschat, A. Dasgupta, G. M. Petrov, and J. L. Giuliani, New J. Phys. **6**, 145 (2004).
[2] G. M. Petrov, J. L. Giuliani, A. Dasgupta, K. Bartschat, and R. E. Pechacek, J. Appl. Phys. **95**, 5284 (2004).
[3] M. Foster, J. L. Peacher, M. Schulz, D. H. Madison, Z. Chen, and H. R. J. Walters, Phys. Rev. Lett. **97**, 093202 (2006).
[4] S. Bellm, J. Lower, K. Bartschat, X. Guan, D. Weflen, M. Foster, A. L. Harris, and D. H. Madison, Phys. Rev. A **75**, 042704 (2007).
[5] J. B. Furness and I. E. McCarthy, J. Phys. B **6**, 2280 (1973).
[6] R. Panajotović, J. Lower, E. Weigold, A. Prideaux, and D. H. Madison, Phys. Rev. A **73**, 052701 (2006).
[7] H. Müller and J. Kessler, J. Phys. B **27**, 5893 (1994).
[8] A. Dorn, A. Elliott, J. C. Lower, S. F. Mazevet, R. P. McEachran, I. E. McCarthy, and E. Weigold, J. Phys. B **31**, 547 (1998).
[9] X. Guo, J. M. Hurn, J. Lower, S. Mazevet, Y. Shen, E. Weigold, B. Granitza, and I. E. McCarthy, Phys. Rev. Lett. **76**, 1228 (1996).
[10] H. Ehrhardt, K. Jung, G. Knoth, and P. Schlemmer, Z. Phys. D: At., Mol. Clusters **1**, 3 (1986).
[11] S. J. Cavanagh, B. Lohmann, J. Rasch, C. T. Whelan, and H. R. J. Walters, Phys. Rev. A **60**, 2977 (1999).
[12] I. Taouil, A. Duguet, A. Lahmam-Bennani, B. Lohmann, J. Rasch, C. T. Whelan, and H. R. J. Walters, J. Phys. B **32**, L5 (1999).
[13] H. T. Prinz, K. H. Besch, and W. Nakel, Phys. Rev. Lett. **74**, 243 (1995).
[14] I. E. McCarthy and E. Weigold, *Electron-Atom Collisions* (Cambridge University Press, Cambridge, England, 1995).
[15] S. Jones, D. H. Madison, and G. F. Hanne, Phys. Rev. Lett. **72**, 2554 (1994).
[16] D. H. Madison, V. D. Kravtsov, S. Jones, and R. P. McEachran, Phys. Rev. A **53**, 2399 (1996).
[17] X. Guo, J. Hurn, J. Lower, S. Mazevet, Y. Shen, I. E. McCarthy, and E. Weigold, in *International Conference on the Physics of Electronic and Atomic Collisions*, Whistler, Canada, edited by L. J. Dubé, J. B. A. Mitchell, J. W. McConkey, and C. E. Brion, AIP Conf. Proc. No. 360 (American Institute of Physics, Woodbury, NY, 1995), p. 795.
[18] S. Mazevet, I. E. McCarthy, and E. Weigold, Phys. Rev. A **57**, 1881 (1998).
[19] G. F. Hanne, Can. J. Phys. **74**, 811 (1996).
[20] D. H. Madison, V. D. Kravtsov, S. Jones, and R. P. McEachran, Can. J. Phys. **74**, 816 (1996).
[21] D. H. Madison, V. D. Kratsov, and S. Mazevet, J. Phys. B **31**, L17 (1998).
[22] S. Bellm, J. Lower, M. Kampp, and C. T. Whelan, J. Phys. B **39**, 4759 (2006).
[23] U. Lechner, S. Keller, E. Engel, H. J. Lüdde, and R. M. Dreizler, in *Electron Scattering from Atoms, Molecules, Nuclei and Bulk Matter*, edited by C. T. Whelan and N. J. Mason (Kluwer, New York, 1997), pp. 239–248.
[24] A. Dorn, A. Elliott, X. Guo, J. Hurn, J. Lower, S. Mazevet, I. E. McCarthy, Y. Shen, and E. Weigold, J. Phys. B **30**, 4097 (1997).
[25] A. Prideaux and D. H. Madison, J. Phys. B **37**, 4423 (2004).
[26] J. Lower, R. Panajotović, S. Bellm, and E. Weigold, Rev. Sci. Instrum. **78**, 111301 (2007).
[27] J. Lower and E. Weigold, J. Phys. E **22**, 4571 (1987).
[28] J. Kessler, in *Polarized Electrons*, 2nd ed., edited by G. Ecker, P. Lambropoulos, and H. Walther (Springer, Berlin, 1985).
[29] A. Prideaux and D. H. Madison, Phys. Rev. A **67**, 052710 (2003).
[30] K. D. Winkler, D. H. Madison, and H. P. Saha, J. Phys. B **32**, 4617 (1999).
[31] H. P. Saha, Phys. Rev. A **53**, 1553 (1996).
[32] D. A. Biava, K. Bartschat, H. P. Saha, and D. H. Madison, J. Phys. B **35**, 5121 (2002).
[33] D. A. Biava, H. P. Saha, E. Engel, R. M. Dreizler, R. P. McEachran, M. A. Haynes, B. Lohmann, C. T. Whelan, and D. H. Madison, J. Phys. B **35**, 293 (2002).
[34] H. P. Saha and D. J. Murray, J. Phys. B **38**, 3015 (2005).
[35] M. Stevenson, G. L. Leighton, A. Crowe, K. Bartschat, O. K. Vorov, and D. H. Madison, J. Phys. B **38**, 433 (2005).
[36] H. P. Saha and D. Lin, Phys. Rev. A **63**, 042701 (2001).